THE JOURNAL OF PHYSICAL CHEMISTRY B LETTERS

**2009,** *113,* 3264–3268
Published on Web 02/25/2009

# Emergence of Superstructures from a Homogeneous Lipid Sphere

**Makiko Negishi,[†] Hiroyuki Kitahata,[‡] and Kenichi Yoshikawa*,[†]**

*Department of Physics, Graduate School of Science, Kyoto University, Kyoto 606-8502, Japan, and Department of Physics, Graduate School of Science, Chiba University, Chiba 263-8522, Japan*

*Received: December 23, 2008; Revised Manuscript Received: February 11, 2009*

The spontaneous generation of a periodic hexagonal superstructure on a giant phospholipid sphere (GPS) with a diameter of 20−200 $\mu$m was studied. The GPS was composed of ternary phospholipids consisting of dioleoylphosphatidylethanolamine (DOPE), dioleoylphosphatidylcholine (DOPC), and dioleoylphosphatidylinositol-bisphosphate ($DOPIP_2$). GPSs were prepared by natural swelling of a lipid film formed on a glass substrate. A GPS with a homogeneous lipid mixture tends to form a two-layered structure between the surface and inner parts; the surface layer is attributed to a $DOPIP_2$ rich region (we call this layer SL), and the interior is rich in DOPE and DOPC (we call this layer IL). A hexagonal superstructure develops in the SL, and the topology then changes to form multiple-doughnut structures. Finally, myelin-like tubes are generated through symmetry breaking of the doughnutlike structures. The time-dependent change in the surface-area expansion of a GPS is shown to obey the logistic growth model, and this is attributed to the kinetic process of phase segregation between the surface and bulk phase of the GPS.

## Introduction

Phospholipid molecules self-assemble into various morphologies, such as vesicles, micelles, hexagonally packed cylinders, and lamellar membrane.[1,2] Especially in a lamellar membrane, several studies have been conducted to reconstitute the biomimetic microdomains.[3,4] Recently, the successes of domain formation in a cell-sized closed artificial membrane consisting of a ternary mixture of sphingomyelin (SM)/dioleoylphosphatidylcholine (DOPC)/cholesterol (Chol)[5−7] or dipalmitoylphosphatidylcholine (DPPC)/DOPC/Chol[8] have been reported. SM and DPPC are saturated phospholipid molecules with zero spontaneous curvature, and DOPC is an unsaturated cylindrical phospholipid molecule. In a mixture of SM/DOPC/Chol or DPPC/DOPC/Chol, Chol produces coexisting liquid-ordered ($L_o$) and liquid-crystalline ($L_\alpha$) phases below the miscibility transition temperature $T_{mix}$.[5−8] Phase separation between $L_o$ and $L_\alpha$ forms a planar micrometer-scale domain in a two-dimensional membrane,[5−8] which can be explained by the theoretical framework of the standard Ginzburg−Landau free-energy functional, coupled with Helfrich's spontaneous curvature model[9] and the line energy of the domain boundaries.[10] In addition to these pioneering works,[5−8] numerical studies have indicated that phase segregation in a ternary mixture of differently shaped phospholipid molecules, which has positive, zero, or negative spontaneous curvature, causes marked morphological changes.[11−14]

Though these pioneering works have reported micrometer-scale pattern formation on a two-dimensional membrane,[3−14] it has not yet been clarified what kind of pattern is formed in a three-dimensional self-assembled system of phospholipid molecules. In this study, we prepared giant phospholipid spheres (GPSs), which were composed of three different phospholipid molecules, dioleoylphosphatidylethanolamine (DOPE) (negative spontaneous curvature), DOPC (cylindrical), and dioleoylphosphatidylinositol-bisphosphate ($DOPIP_2$) (positive spontaneous curvature). Here, we adopted the term GPS as the sphere filled with phospholipid molecules. DOPE is an inverted-cone-shaped molecule with an intrinsic curvature of $-0.48$ $nm^{-1}$,[15] and phosphatidylethanolamine (PE) can comprise as much as 70−80% of the total phospholipid molecules in *Escherichia coli*.[16] DOPC is a cylindrical-shaped molecule with an intrinsic curvature of $-0.11$ $nm^{-1}$,[15] and phosphatidylcholine constitutes more than 50% of the total phospholipid molecules in mammalian plasma membrane.[17] $DOPIP_2$ is a cone-shaped molecule that has unique physicochemical properties because of its large headgroup, an inositol ring with two phosphate substrates. The inositol ring extends directly into the aqueous phase from the membrane surface, to permit maximum hydration, and its orientation/conformation can be modified by interactions with biological molecules and the composition of the membrane.[18] Phosphatidylinositol-bisphosphate ($PIP_2$) is an important phospholipid molecule in biology. $PIP_2$ participates in endocytosis and exocytosis, and is a critical second messenger that plays a role in various cellular activities including modulation of the actin cytoskeleton, focal adhesion formation, and nuclear events.[19,20] Here, we report that a micrometer-scale periodic superstructure evolves on the surface of a GPS (early stage), and as a successive phenomenon, a topological change is induced (late stage).

## Materials and Methods

**Materials.** 1,2-Dioleoyl-*sn*-glycero-3-phosphoethanolamine (DOPE), 1,2-dioleoyl-*sn*-glycero-3-phosphocholine (DOPC), 1,2-dioleoyl-*sn*-glycero-3-[phosphoinositol-4,5-bisphosphate] ($DOPIP_2$),

* Corresponding author. Phone: +81 75 753 3812. Fax: +81 75 753 3779. E-mail: yoshikaw@scphys.kyoto-u.ac.jp.
[†] Kyoto University.
[‡] Chiba University.

10.1021/jp8113623 CCC: $40.75 

1-oleoyl-2-[12-[(7-nitro-2-1,3-benzoxadiazol-4-yl)amino]dodecanoyl]-*sn*-glycero-3-phosphoethanolamine (NBD-PE), and 1-oleoyl-2-[12-[(7-nitro-2-1,3-benzoxadiazol-4-yl)amino]dodecanoyl]-*sn*-glycero-3-phosphocholine (NBD-PC) were purchased from Avanti Polar Lipids, Inc. 2-[4-(2-Hydroxy-ethyl)-1-piperazinyl]ethanesulfonic acid (HEPES) was obtained from Dojin Chemical Co. All chemical compounds were used without further purification.

**Preparation of GPSs.** GPSs were formed spontaneously by the natural swelling of a lipid film. DOPE was dissolved in chloroform at a concentration of 10 mM. DOPC was dissolved in a chloroform/methanol (2:1, v/v) mixture at a concentration of 10 mM. $DOPIP_2$ was dissolved in a chloroform/methanol (3:1, v/v) mixture at a concentration of 2.5 mM. 1 $\mu$mol portion (total lipid amounts) of binary or ternary mixed phospholipids was dried up by spraying with nitrogen gas very rapidly, in order to prepare a uniform mixture of lipid film. After that, the lipid film was evaporated for 10 min to remove the organic solvent completely. We have confirmed that, through the procedure on the rapid evaporation of the organic solvent, reproducible results were obtained, whereas a nonuniform and walleyed lipid film by the slow evaporation did not give GPSs with a superstructure. Special care was taken to prevent the contamination of impurities such as $Ca^{2+}$ during the sample preparation. 23 different phospholipid mixtures were examined. To observe the distribution of DOPE and DOPC in a GPS, NBD-PE and NBD-PC were included in a lipid mixture. We always kept the relative ratio of the total fluorescent-labeled lipids, NBD-PE plus NBD-PC, with respect to the total unlabeled lipids, DOPE and DOPC, to be constant as 0.05 mol %. The dry lipid films were hydrated with 100 mM HEPES buffer solution (pH 7.5) for 60 min at 50 °C, and GPSs were spontaneously generated in HEPES buffer solution in a well-dispersed state. Immediately after hydration, the solution was kept at 20 °C.

**Observation of GPSs.** An observation chamber was made with double-sided adhesive tape (less than 0.5 mm thick) with a cylindrical hole (8 mm diameter) fixed on a microscopic cover-glass slide (Matsunami Glass Ind., Ltd.). Glass slides had been previously cleaned by baking for 1 h at 500 °C. 5 $\mu$L portion of the solution containing GPSs was placed at the center of the cylindrical hole in the tape, and another cover-glass was fixed on the top of the double-sided adhesive tape. GPSs were observed under a confocal laser-scanning microscope (LSM 510, Carl Zeiss, Inc.) with the 458 nm beam of an argon laser. In each condition, 50−70 GPSs could be observed in the specimen on the glass slide. All experiments were carried out several times at a given lipid composition to confirm the reproducibility of the observation. We performed the observation on the superstructure formation with/without NBD-PE and with/without NBD-PC to check the effect of these fluorescence probes. We found that there was no essential difference on the superstructure formation.

## Results and Discussion

**Morphological Variation.** According to the results of systematic observations, the morphologies are summarized in a phase diagram in Figure 1A. After GPSs were prepared by natural swelling at 50 °C for 60 min, the sample solution was left at 20 °C for 120 min. At low concentrations of DOPC (the yellow region in Figure 1A), any apparent structural objects were not observed under our microscopic condition. The $DOPIP_2$/DOPC mixture formed various morphologies according to the molar ratio of $DOPIP_2$/DOPC. For $DOPIP_2$/DOPC = [10/0], [9/1], [8/2], and [7/3], GPSs with a homogeneous smooth

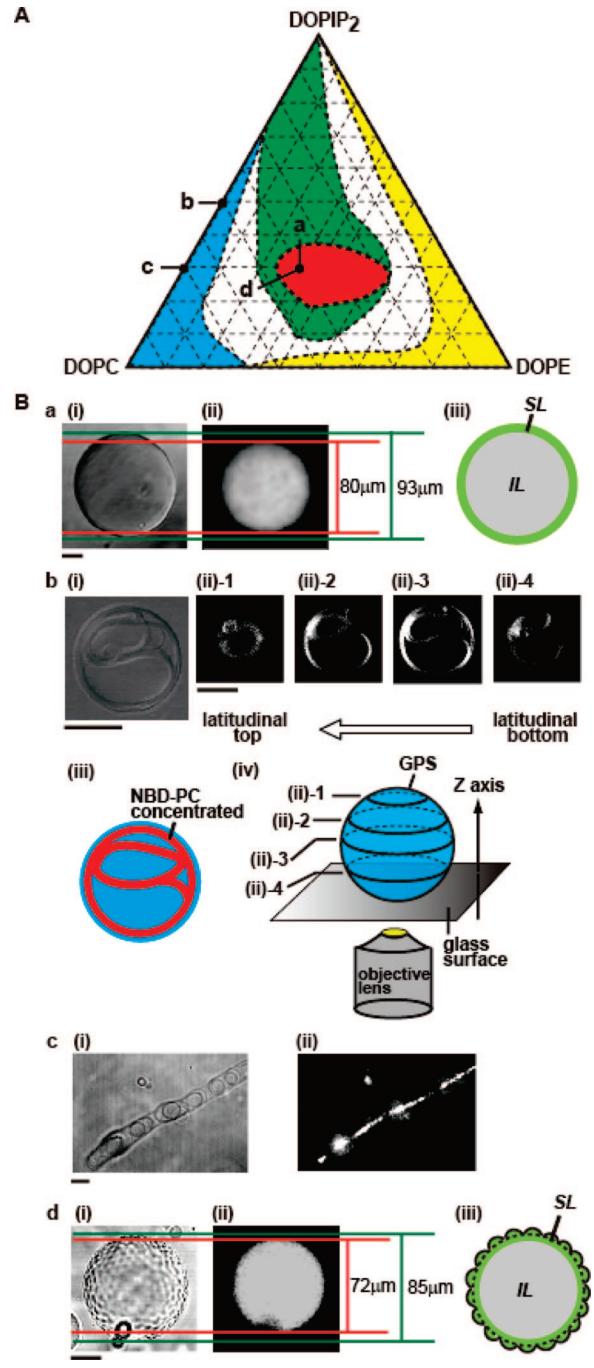


**Figure 1.** (A) Phase diagram of the relation between phospholipid composition and micrometer-scale structure. The green region in part A indicates that GPSs with a homogeneous surface appeared, immediately after natural swelling. In the blue region, tubelike structures encapsulated within a transparent film were observed (see Supporting Information Figure S1). The red region indicates the generation of GPSs with superstructure on its surface. In the yellow region, any optical visible structure was not found. Symbols a−d in part A correspond to $DOPIP_2$/DOPE/DOPC = [3/3/4], [5/0/5], [3/0/7], and [3/3/4], respectively. (B) Typical images at each coordinate for a−d in part A. a(i)−d(i) are transmission images, and a(ii)−d(ii) are confocal fluorescence images of a(i)−d(i), respectively. a(iii), b(iii), and d(iii) are schematic images. The white structure in a(ii) and d(ii) is the fluorescence from both NBD-PE and NBD-PC, and that in b(ii) and c(ii) is fluorescence from NBD-PC. The focus is on the equator of a GPS parallel to the glass surface (except b(ii)). In b(ii), the focus is moved latitudinally from the top ((ii)-1) to the bottom ((ii)-4) of the spherical structure indicated in b(i). b(iv) is a schematic illustration of the focus for (ii)-1 to (ii)-4. The wavenumber ($q$) of the periodic superstructure in d(i) is 0.11 $\mu m^{-1}$. The scale bars are 20 $\mu$m.

surface were observed, as in Figure 1B-a. With a decrease in the molar ratio of $DOPIP_2$, two characteristic morphologies appeared, as shown in Figures 1B-b and c. In $DOPIP_2$/DOPC = [5/5], a tube structure packed inside a spherical object was generated, where NBD-PC probes were localized on a tube structure (Figure 1B-b together with Supporting Information Figure S1). In $DOPIP_2$/DOPC = [7/3], a longitudinally extended tube structure, in which NBD-PC species were localized, was wrapped by the other layer structure (Figure 1B-c).

In the ternary mixture of $DOPIP_2$/DOPE/DOPC, GPSs with a smooth and homogeneous surface were invariably observed. When NBD-PE and NPD-PC fluorescence probes were mixed with a sample, the probes were localized in the inner volume of a GPS. Therefore, we consider that the surface layer of a GPS is rich in $DOPIP_2$ (we call this layer SL), and the interior is rich in both DOPE and DOPC (we call this layer IL) (Figure 1B-a). In the red region in Figure 1A, some GPSs exhibited a periodic hexagonal superstructure on their surfaces (Figure 1B-d). When the solution temperature was maintained at 50 °C, a periodic superstructure did not appear on the surface of GPSs. The average percentage of GPSs with a periodic superstructure for $DOPIP_2$/DOPE/DOPC = [3/3/4], [3/3.5/3.5], [3/4/3], [2.5/3.5/4], [3/5/2], or [2/4/4] is 23, 15, 9, 19, 4, or 3%, respectively. Thus, a periodic superstructure was most likely to be generated on a GPS surface for the [3/3/4] mixture. For [2/4/4], [3/5/2], and [3/4/3], the average percentages of GPSs with a periodic superstructure were less than 10% of the total GPSs. In these experiments, a periodic superstructure developed when the diameter was greater than 20 $\mu$m.

**Time Evolution of a Periodic Hexagonal Superstructure.** As shown in Figure 2, the statistical average of the wavenumber $q$ for a periodic superstructure on [3/3/4] GPSs decreased with time at 20 °C. The wavenumber $q$ was calculated from the characteristic length $L$ (Figure 3B) of the outermost superstructure on a GPS transmission image where the focus was the equator of the GPS parallel to the glass surface.

Figure 3A summarizes the time-dependent change in morphology for a GPS. First, a small periodic hexagonal superstructure was formed on the uppermost surface of the GPS (Figure 3A-a, $q = 0.11\ \mu m^{-1}$, $h = 2.6\ \mu$m), and the superstructure gradually grew both longitudinally and laterally (Figure 3A-b, $q = 0.067\ \mu m^{-1}$, $h = 5.7\ \mu$m). Next, the center of each hexagon began to sag downward, to give a multiple-doughnut structure (Figure 3A-c, $q = 0.037\ \mu m^{-1}$, $h = 9.7\ \mu$m) (topological change). Finally, a tubelike structure was generated through symmetry breaking of the doughnutlike structure (Figure 3A-d, $q = 0.028\ \mu m^{-1}$, $h = 14.4\ \mu$m). The valley-to-valley distances for two kitty-cornered hexagonal $R_{v-v}$ (Figure 3B) and for the IL $R_{IL}$ (Figure 3B) are 183 and 177 $\mu$m for Figure 3A-a and 177 and 177 $\mu$m for Figure 3A-c, respectively. When $R_{v-v}$ was nearly equal to $R_{IL}$, the topological change started. We refer to the stages before and after the initiation of the topological change the early stage and late stage, respectively.

Figure 3C shows the time-dependent growth of $q$ for a superstructure on a GPS. The plot clearly shows that the power law of the late stage is different from that of the early stage. Although repeated experiments to estimate the time evolution of a superstructure on a GPS (data not shown) indicate that the exponent of the growth law in the early stage depended on the GPS, the time evolution was always divided into an early stage and late stage, and the topological change was always observed in the late stage.

Figure 3D indicates the time-dependent expansion of the surface area $\Delta A$ on the GPS given in Figure 3A. The plot

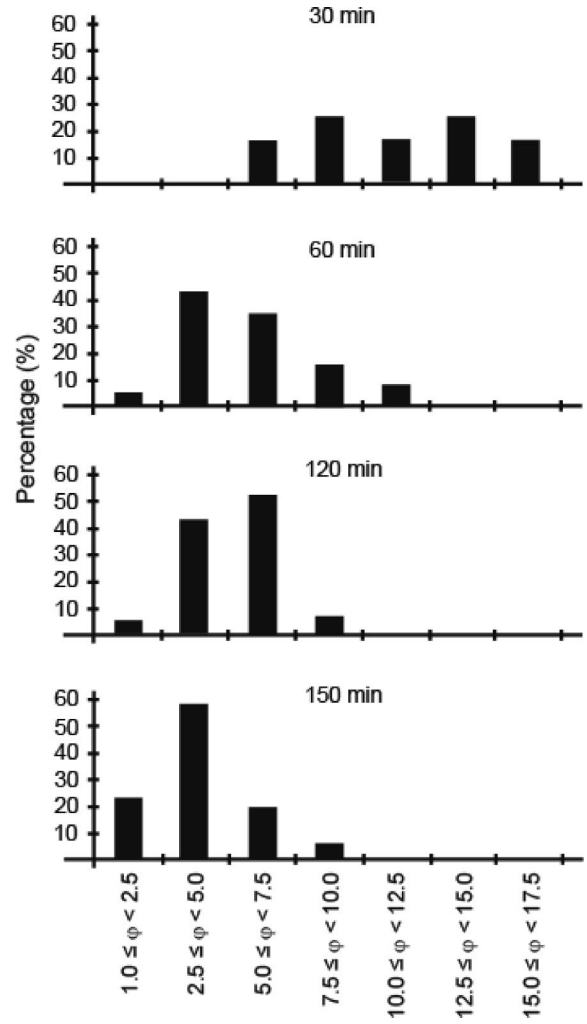


**Figure 2.** Estimation of the statistical average of wavenumber $q$. All GPSs for this analysis consisted of a $DOPIP_2$/DOPC/DOPE = [3/3/4] mixture. An estimated 50−70 GPSs were seen in sample solutions that were kept at 20 °C for 30, 60, 120, or 150 min after the natural swelling at 50 °C. The number of GPSs with a periodic hexagonal superstructure among total GPSs was as follows: 12 at 30 min, 19 at 60 min, 23 at 120 min, and 23 at 150 min. The horizontal axis is $\varphi = q \times R_{v-v}$ to normalize the difference in radius for each GPS.

shows a typical logistic curve throughout the process of superstructure evolution. The surface area of the GPS rapidly increases in the early stage, and the growth reaches a plateau that coincides with the beginning of the qualitative change in the surface structure.

After 4 h from sample preparation, GPSs with a superstructure exhibited completely symmetry breaking, as shown in Figure 4 and Supporting Information Figure S2. Longitudinally extended myelin-like tube structures were protruded from the GPS with the localization parts of NBD-PE and NPD-PC at its central axis (Figure 4B). In the IL, onionlike structures were observed, where both NBD-PE and NBD-PC were highly concentrated.

As shown in Figure 3D, the time course of the change in the surface area is characterized with three different steps of an initial slow stage, an intermediate fast change, and finally a slow change with asymptotic behavior. Thus, we tried to fit the experimental data regarding the kinetics of surface-area expansion with a simple differential equation consisting of a polynomial expression with first- and second-order terms. As shown

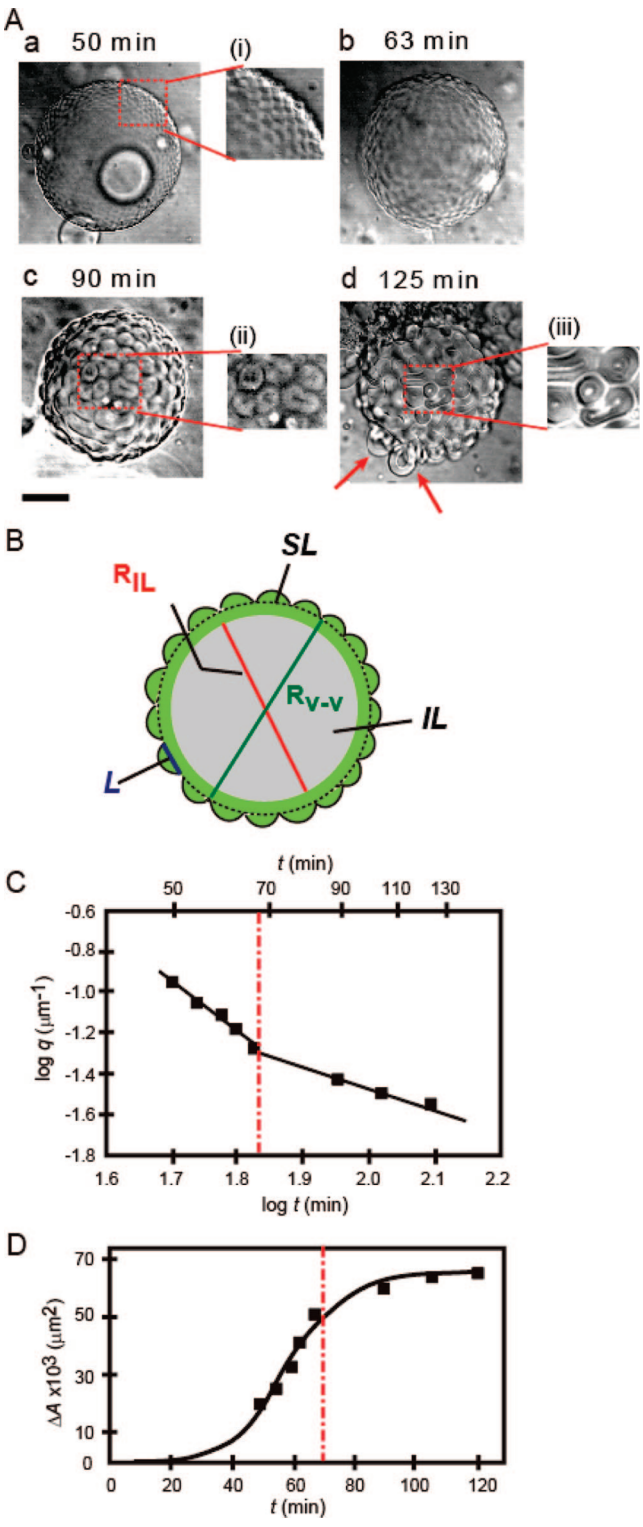


**Figure 3.** Time evolution of the superstructure on a GPS. (A) Transmission images where the focus is on the equator of a GPS parallel to the glass slide: (a) the image at 50 min after the GPS is held at 20 °C, (b) 63 min, (c) 90 min, and (d) 125 min, respectively. The red arrows in d indicate tubelike structures. The scale bar is 50 $\mu$m. (i)−(iii) Enlarged images of superstructures at 50, 90, and 125 min, respectively. (B) Schematic image. (C) Log−log plot of the time evolution of superstructures of the GPS depicted in part A. The horizontal axis is the wavenumber $q$, and the vertical axis is the time $t$ after the quenching. For 50 min $\leq t \leq$ 67 min (early stage), $\log q = -2.5 \log t + 3.4$, and for $t \leq 67$ (late stage), $\log q = -1.0 \log t + 0.59$. (D) The plot of the surface area $\Delta A$ versus time $t$. $\Delta A = 64677.0/(1 + \exp 0.11(t_0 - t))$. The red dashed line in parts C and D indicates the transition time from the early stage to the late stage.

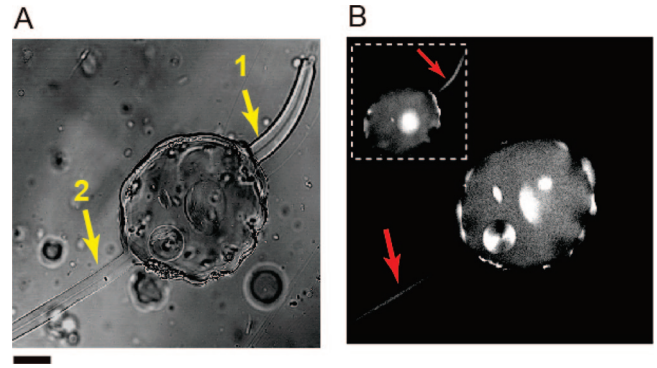


**Figure 4.** Example of microscopic images of a GPS, $DOPIP_2$/DOPC/DOPE = [3/3/4], after 4 h. The focal plane is on the equator of the GPS parallel to the glass slide. (A) Transmission image. The yellow arrows indicate myelin-like tubes. (B) Confocal fluorescence image (inset: the focal plane was ca. 20 $\mu$m below the equator parallel to the glass slide). The white part in part B corresponds to the fluorescence from NBD-PE and NBD-PC. The central axis of the myelin-like tubes is the localized region of NBD-PE and NBD-PC (red arrows). The scale bar is 50 $\mu$m.

in Figure 3D, the experimental trend is reproduced in a rather satisfactory manner.

$$\frac{d(\Delta A)}{dt} = \mu \Delta A - \eta(\Delta A)^2 \quad (1)$$

where the first term on the right indicates a positive-feedback process with the simplest approximation, which is called a logistic growth model. The kinetic equation given by eq 1 has frequently been used as a basic model for many biological growth processes such as tumor cell growth[20,22] and the development of brain cortical convolutions.[23]

In general, it is known that phase segregation can be expressed in terms of autocatalytic kinetics for the initial stage. Although we have not obtained detailed information on the mechanism of the occurrence of the superstructure yet, we expect that the seemingly autocatalytic kinetics, as in the first term in eq 1, reflects the time-dependent growth of micro-phase segregation. The rapid change after the initial slow process implies the existence of a cooperative phenomenon, i.e., phase segregation of the lipid mixture. Our observation indicates that the phase segregation occurs at the interface between the surface of the GPS and the bulk parts during the early stage. After the initial process of the morphological change (in the late stage), multiple-doughnut and tube structures are induced on the GPS, and the growth of the surface area (Figure 3D) reaches a plateau, where the time-dependent change in the surface area reaches a minimum.

## Conclusion

We observed the time development of a superstructure on a spherical object formed in ternary mixtures of $DOPIP_2$/DOPE/DOPC, where the lipid molecules are characterized with the head groups of large, small, and intermediate sizes. The expansion of the surface area of the superstructure with time follows the logistic growth model. We consider that the physicochemical origin of this process can be attributed to the phase segregation between the surface and bulk phase of a solution of spherical objects. We also found that, after the initial development of the hexagonal superstructure, new morphologies, such as a multiple-doughnut and tube, appear in the late stage.

**Acknowledgment.** We thank Prof. H. Seto and Dr. Y. Takenaka for fruitful discussions. This work was supported by a Grant-in-Aid for Creative Scientific Research (18GS0421) and a Grant-in-Aid for Scientific Research on Priority Areas (17076007) from the Ministry of Education, Culture, Sports, Science and Technology of Japan.

**Supporting Information Available:** Typical examples of tube structures packed in a sphere with the composition of $DOPIP_2/DOPC = [5/5]$ (Figure S1), and typical transmission images on the formation of longitudinally extended myelin-like tubes emerged from a sphere in $DOPIP_2/DOPC/DOPE = [3/3/4]$ (Figure S2). This material is available free of charge via the Internet at http://pubs.acs.org.

## References and Notes

(1) Hoffmann, H.; Ebert, D. H. G. *Angew. Chem., Int. Ed. Engl.* **1988**, *27*, 902–912.
(2) Ces, O.; Mulet, X. *Signal Transduction* **2006**, *6*, 112–132.
(3) Gege, C.; Schneider, M. F.; Schumacher, G.; Limozin, L.; Rothe, U.; Bendas, G.; Tanaka, M.; Schmidt, R. R. *ChemPhysChem* **2004**, *5*, 216–224.
(4) Purrucker, O.; Frtig, A.; Ldtke, K.; Jordan, R.; Tanaka, M. *J. Am. Chem. Soc.* **2005**, *127*, 1258–1264.
(5) Baumgart, T.; Hess, S. T.; Webb, W. W. *Nature* **2003**, *425*, 821–824.
(6) Veatch, S. L.; Keller, S. L. *Phys. Rev. Lett.* **2005**, *94*, 148101.
(7) Rozovskt, S.; Kaizuka, Y.; Groves, J. T. *J. Am. Chem. Soc.* **2005**, *127*, 36–37.
(8) Veatch, S. L.; Keller, S. L. *Biophys. J.* **2003**, *85*, 3074–3083.
(9) Helfrich, W. *Z. Naturforsch.* **1973**, *28C*, 693–703.
(10) Jülicher, F.; Lipowsky, R. *Phys. Rev. E* **1996**, *53*, 2670.
(11) Jiang, Y.; Lookman, T.; Saxena, A. *Phys. Rev. E* **2000**, *61*, R57.
(12) Taniguchi, T. *Phys. Rev. Lett.* **1996**, *76*, 4444.
(13) Kumar, P. B. S.; Gompper, K. G.; Lipowsky, R. *Phys. Rev. E* **1999**, *60*, 4610.
(14) MacKintoxh, F. C.; Safran, S. A. *Phys. Rev. E* **1993**, *47*, 1180.
(15) Hamai, C.; Yang, T.; Kataoka, S.; Cremer, P. S.; Musser, S. M. *Biophys. J.* **2006**, *90*, 1241–1248.
(16) Dowhan, W. *Annu. Rev. Biochem.* **1997**, *66*, 199–232.
(17) Yechiel, E.; Barenholz, Y. *J. Biol. Chem.* **1985**, *260*, 9123–9131.
(18) Bradshaw, J. B.; Bushby, R. J.; Giles, C. C. D.; Saunders, M. R.; Reid, D. G. *Nat. Struct. Biol.* **1996**, *3*, 125–127.
(19) Czech, M. P. *Annu. Rev. Physiol.* **2003**, *65*, 791–815.
(20) Doughman, R. L.; Firestone, A. J.; Anderson, R. A. *J. Membr. Biol.* **2003**, *194*, 77–89.
(21) Ai, B. Q.; Wang, X. J.; Liu, G. T.; Liu, L. G. *Phys. Rev. E* **2003**, *67*, 022903.
(22) Wang, C. J.; Wei, Q.; Mei, D. C. *Phys. Lett. A* **2008**, *372*, 2176–2182.
(23) Toro, R.; Burnod, Y. *Cereb. Cortex* **2005**, *15*, 1900–1913.

JP8113623